Heliyon 9 (2023) e20718

Contents lists available at ScienceDirect

Heliyon

journal homepage: www.cell.com/heliyon

A novel clinical-radscore nomogram for predicting ruptured intracranial aneurysm

Wenjie Li [1], Xiaojia Wu [1], Jing Wang, Tianxing Huang, Lu Zhou, Yu Zhou, Yuanxin Tan, Weijia Zhong **, Zhiming Zhou *

Department of Radiology, The Second Affiliated Hospital of Chongqing Medical University, Chongqing, 400010, China

ARTICLE INFO

Keywords:
Computed tomography angiography
Inflammatory marker
Radiomics features
Rupture
Intracranial aneurysm

ABSTRACT

Objectives: Our study aims to find the more practical and powerful method to predict intracranial aneurysm (IA) rupture through verification of predictive power of different models.

Methods: Clinical and imaging data of 576 patients with IAs including 192 ruptured IAs and matched 384 unruptured IAs was retrospectively analyzed. Radiomics features derived from computed tomography angiography (CTA) images were selected by *t*-test and Elastic-Net regression. A radiomics score (radscore) was developed based on the optimal radiomics features. Inflammatory markers were selected by multivariate regression. And then 4 models including the radscore, inflammatory, clinical and clinical-radscore models (C–R model) were built. The receiver operating characteristic curve (ROC) was performed to evaluate the performance of each model, PHASES and ELAPSS. The nomogram visualizing the C–R model was constructed to predict the risk of IA rupture.

Results: Five inflammatory features, 2 radiological characteristics and 7 radiomics features were significantly associated with IA rupture. The areas under ROCs of the radscore, inflammatory, clinical and C–R models were 0.814, 0.935, 0.970 and 0.975 in the training cohort and 0.805, 0.927, 0.952 and 0.962 in the validation cohort, respectively.

Conclusion: The inflammatory model performs particularly well in predicting the risk of IA rupture, and its predictive power is further improved by combining with radiological and radiomics features and the C–R model performs the best. The C–R nomogram is a more stable and effective tool than PHASES and ELAPSS for individually predicting the risk of rupture for patients with IA.

Abbreviations: AUC, areas under the curves; C–R, clinical-radscore; CTA, computed tomography angiography; DCA, decision curve analysis; ECM, extracellular matrix; hs-CRP, hypersensitive c-reactive protein; IA, intracranial aneurysm; ICC, interclass correlation coefficient; Radscore, radiomics score; ROC, receiver operating characteristic curve; ROI, region of interest; SAH, subarachnoid hemorrhage; WBC, white blood cell count; WSS, wall shear stress.

* Corresponding author. Department of Radiology, The Second Affiliated Hospital of Chongqing Medical University, Chongqing, 400010, China.
** Corresponding author.
E-mail addresses: zhongwj@cqmu.edu.cn (W. Zhong), zhouzhiming1127@cqmu.edu.cn (Z. Zhou).

[1] Wenjie Li and Xiaojia Wu contributed to the work equally and should be regarded as co-first authors.

https://doi.org/10.1016/j.heliyon.2023.e20718
Received 2 June 2023; Received in revised form 2 October 2023; Accepted 4 October 2023
Available online 5 October 2023

1. Introduction

Rupture of intracranial aneurysm (IA) is the first cause of nontraumatic subarachnoid hemorrhage (SAH) with an incidence of 3–7% in the population [1]. Although there is only a low risk of rupture with 9‰ annually [2], the mortality is as high as 65% [3]. Due to disastrous injury to patients after IA rupture, timely treatment is necessary. Surgical or intravascular treatment of IAs is proven to be effective [4]. Early identification of IAs with high risk of rupture is critical to help timely perform an intervention for prevention of rupture.

Previous studies have confirmed a large number of predictors including demographic, genetic, morphology, hemodynamic and inflammatory characteristics, are associated with the rupture of IA [5–7]. On this basis, the PHASES score and the ELAPSS score, which are composed of size, location, and shape, gender, history of hypertension, population and personal or family history of SAH, are two scales used in clinical work to assess the risk of growth and rupture of unruptured IAs [8,9]. However, these two scales have very limited predictive power in predicting the rupture of IAs [10,11]. In terms of the predictors of the scales, the inclusion of more comprehensive or quantitative information related to IAs, such as inflammatory or radiomics features, may be helpful in predicting the risk of IA rupture.

Inflammation factors play a very important role in the development of IAs [12]. The accumulating evidences have revealed that the peripheral blood inflammatory indexes, such as platelet-to-WBC ratio, platelet-to-neutrophil ratio, or neutrophil-to-lymphocyte ratio, have critical clinical value as new biomarkers for predicting IA rupture [13,14]. Radiomics is a high-throughput technology that can extract massive features from image data, which can provide information for diagnosis, prognosis and treatment response [15]. In recent years, several studies have found that some radiomics features of IAs, such as Elongation and Flatness, are different between ruptured and unruptured IAs, and the models that incorporate radiomics features usually achieve better performances [16–18]. Thus, further evaluation of predictive performance of IA rupture through analysis of inflammatory and radiomics features is valuable. However, to our knowledge, there are very few such studies.

Therefore, our study aims to analyze peripheral blood inflammatory indexes and radiological characteristics and radiomics features between ruptured and unruptured IAs and try to establish a powerful and practical predictive nomogram combined with the radiomics and inflammatory and radiological characteristics to predict IA rupture.

2. Methods

2.1. Patients

This retrospective study was approved by our hospital's Human Experimentation Ethical Standards Committee, and written informed consent was obtained from each participant.

We reviewed 1567 patients diagnosed with IA by computed tomography angiography (CTA) or digital subtraction angiography at 2 centers in our hospital from January 2015 to November 2021. The exclusion criteria included: (1) secondary IAs or IAs combined with intracranial vascular diseases; (2) the maximum diameter of IAs <2 mm; (3) multiple or fusiform IAs; (4) IAs that was indistinguishable from infundibulum; (5) interventional therapy or surgery for IAs before CTA; (6) poor-quality images of CTA.

2.2. Demographic and clinical data

Demographic data, clinical (radiological and inflammatory) characteristics of each participant were collected from our hospital's information system. The demographic information included age, gender, history of coronary heart disease, hypertension, and diabetes, smoking history and alcohol consumption, current and previous history of transient ischemic attack or ischemic stroke, history of arterial stenosis, recent use of aspirin and lipid-lowering drugs, family history of SAH and previous history of SAH.

Inflammatory characteristics of the followings were collected: the absolute and percentage of neutrophils, lymphocytes, monocytes and eosinophils, the total number of platelets, white blood cell count (WBC), hypersensitive c-reactive protein (hs-CRP) and c-reactive protein [12].

The implementation of PHASE and ELAPSS followed protocols of previous studies [8,19].

2.3. Random sampling

In order to balance the number of ruptured and unruptured IAs, we used a random number seed method to randomly select patients as twice number as ruptured IAs from the unruptured IAs as a control group. Then, the Mann-Whitney *U* test was performed for PHASES of selected samples and population.

Finally, the patients with ruptured and unruptured IAs were randomly divided into training and validation cohorts by computer software in a ratio of 7:3.

2.4. CTA examinations and image analysis

Head CTA examinations were performed with multislice CT scanners (Siemens Healthcare, Somatom Definition Force, Canon medical Systems and Aquilion ONE). The protocol of CTA were as follows: 200–250 mA, 110–120 kV, 1-mm layer thickness, 0.7-mm layer spacing, and 512 $\times$ 512 matrix. A total dose of 150–300 mg/kg of contrast agent (iohexol solution) was injected at a flow rate of

4.5–5.0 ml/s.

Before image analysis, we preprocessed the images as follows: (1) the CTA data were resampled to 1.0 × 1.0 × 1.0 mm^3 voxel size; (2) gray level discretization were resampled on a fixed number of 256 bins; (3) the CTA images were set to a window level of 50 Hounsfield unit (Hu) and window width of 110 Hu. We obtained standard head CTA images on the axial section, and used the 3-dimensional volume rendering (3D-VR), maximum intensity projection (MIP) and multi-plane reformation (MPR) views for post-processing reconstruction and measurement.

Eight radiological characteristics were recorded, including IAs' size, shape (regular or irregular, daughter sacs, lobulated, non-smooth and bulge), presence or absence of branching vessels, location (internal carotid, anterior cerebral/anterior communication, middle cerebral and posterior circulation/posterior communication), major axis length, minor axis length, base width and parent artery diameter [1,5]. Two radiologists independently analyzed the images without knowing the patient's clinical status, and then finally reached a consensus.

Two radiologists used the ITK-SNAP software (version 3.8.0) to generate manual region of interest (ROI) on a per-slice basis on the original axial, reconstructed coronal, and sagittal CTA images. The ROI contained the entire lesion volume.

2.5. Radiomics analysis

The workflow of radiomics analysis is shown in Fig. 1, including image acquisition, ROI segmentation, feature extraction, feature selection, model construction and evaluation.

Radiomics features extraction: After the ROIs segmentation, the radiomics features were automatically extracted by Python software (version 3.2) from 8 feature groups including neighborhood gray level dependency matrix (GLDM), neighborhood gray difference matrix (NGTDM), gray level run length matrix (GLRLM), gray level size zone matrix (GLSZM), gray level co-occurrence matrix (GLCM), 2D shape, 3D shape, and first-order statistics. Totally 107 radiomics features were gained from each IA.

Reproducibility analysis of radiomics features: Data from randomly selected 50 cases in the training cohort was used for inter-observer and intra-observer reproducibility assessment. The ROIs of each patient was semi-automatically segmented again by the same radiologist with 7-days interval and by another trained radiologist using the same method. The interclass correlation coefficient (ICC) was employed for assessment of inter-observer and intra-observer agreement.

Harmonization of radiomics features: after radiomics features extraction, harmonization in the feature domain was performed. First, variables with zero variance were excluded, and the missing values were replaced by the median. Then the data were standardized by the Standard Scaler function of Python software.

Radiomics feature selection: Python software was used to select the radiomics features. Among 107 radiomics features, the independent samples *t*-test and Elastic-Net regression were used to select the radiomics features that were most associated with the rupture of IAs in the training cohort.

2.6. Model construction

In the training cohort, the independent risk factors ($P < 0.05$) of demographic data, radiological and inflammatory characteristics of IA rupture were tested by univariate analysis and multivariate logistic regression. We used significant independent inflammatory features to establish an inflammatory model by logistic regression. The radiological features and inflammatory features were combined to construct the clinical model. The radiomics model was constructed by using the optimal radiomics features and their coefficients in the Elastic-Net regression.

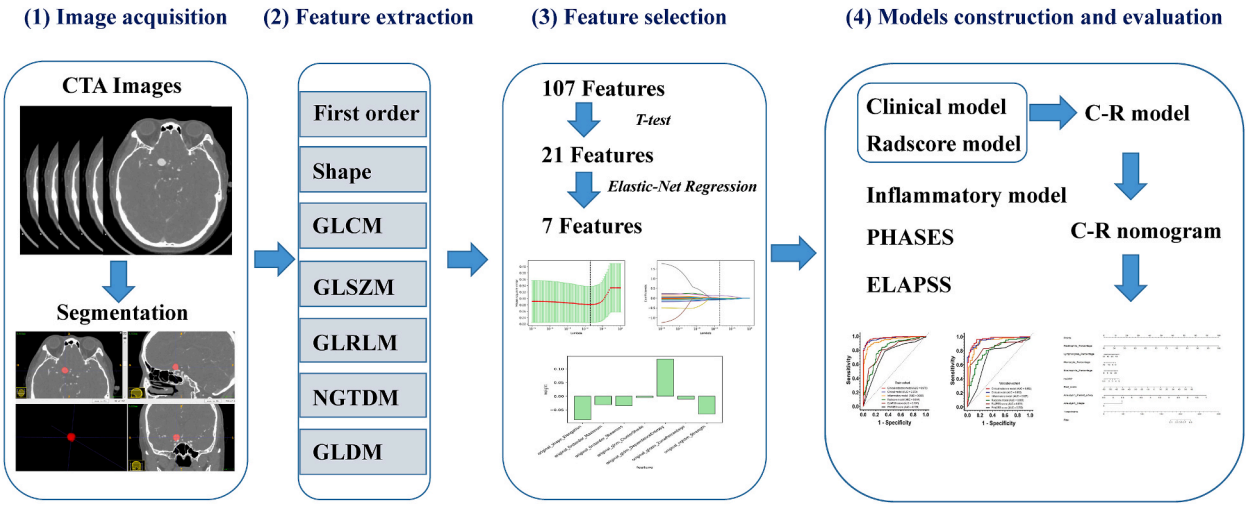

Fig. 1. Workflow of radiomics analysis for predicting IA rupture.

We combined the clinical model with the radscore model to construct the clinical-radscore (C–R) model. Finally, a multi-predictor nomogram, which incorporated clinical and radiomics risk factors, was constructed through the multivariate logistic regression. We independently verified those models in the validation cohort, and evaluated the performance of each model by calculating the area under the curve (AUC).

2.7. Model evaluation

We used receiver operating characteristic (ROC) analysis to evaluate the differentiation performance of each model and calculated the specificity, sensitivity, accuracy, and AUC of each model. The DeLong test were used to compare the AUCs between different models. We used calibration curve analysis and decision curve analysis (DCA) to evaluate the calibration ability and clinical usefulness of the C–R nomogram, respectively.

2.8. Statistical analysis

Statistical analysis was performed by R software (version 3.6.0). Variables were described by mean ± standard deviation, median (interquartile range) or counts (percentages). The Kolmogorov-Smirnov test was performed to check the normality of continuous variables. The Mann-Whitney *U* test, Student's t-test, chi-square test or Fisher exact test were performed to determine the between-group differences. A value of $P < 0.05$ was considered statistically significant.

Table 1
Patients' characteristics in the training and validation cohorts.

Variables	Training Cohort (n = 403)	Validation Cohort (n = 173)	*P* value
Age (y)	63.00 [53.00–71.00]	62.00 [52.00–71.00]	0.791
Male	165 (40.9%)	75 (43.4%)	0.591
Proximal diameter of parent artery (mm)	3.20 [2.40–3.80]	3.20 [2.40–3.80]	0.733
Base width (mm)	2.70 [2.20–3.40]	2.70 [2.20–3.45]	0.721
Minor axis (mm)	2.60 [1.80–3.70]	2.50 [1.80–3.95]	0.426
Major axis (mm)	3.20 [2.20–4.80]	3.30 [2.35–5.10]	0.318
Irregular shape	71 (17.6%)	36 (20.8%)	0.367
Regular shape	332 (82.4%)	137 (79.2%)	0.367
Branching vessels	103 (25.6%)	33 (19.1%)	0.093
Internal carotid artery	280 (69.5%)	119 (68.8%)	0.810
Anterior communicating artery	48 (11.9%)	24 (13.9%)	0.810
Middle cerebral artery	48 (11.9%)	17 (9.8%)	0.810
Posterior cerebral artery	27 (6.7%)	13 (7.5%)	0.810
PLT (10^9/L)	197.15 ± 66.12	204.27 ± 62.25	0.228
C-reactive protein	5.00 [5.00–5.68]	5.00 [5.00–6.54]	0.101
WBC (10^9/L)	6.70 [5.23–10.00]	8.04 [6.14–10.95]	0.001
Hs-CRP (mg/L)	1.74 [0.54–5.00]	2.14 [0.73–5.00]	0.217
Monocyte percentage (%)	5.68 ± 2.51	5.60 ± 2.80	0.723
Monocyte count (10^9/L)	0.39 [0.29–0.51]	0.41 [0.29–0.57]	0.259
Lymphocyte percentage (%)	19.80 [8.90–28.10]	18.40 [7.60–26.95]	0.243
Lymphocyte count (10^9/L)	1.21 [0.86–1.67]	1.23 [0.79–1.77]	0.828
Eosinophil percentage (%)	0.90 [0.10–2.10]	0.80 [0.10–2.00]	0.147
Eosinophil count (10^9/L)	0.06 [0.01–0.13]	0.05 [0.01–0.13]	0.371
Neutrophil percentage (%)	71.50 [62.30–86.10]	73.10 [64.25–87.90]	0.166
Neutrophil count (10^9/L)	4.57 [3.26–8.74]	5.63 [4.04–9.00]	0.003
Smoking history	100 (24.8%)	49 (28.3%)	0.378
Hypertension	243 (60.3%)	103 (59.5%)	0.864
Recent Aspirin Use< 3 weeks	6 (1.5%)	6 (3.5%)	0.291
Recent Aspirin Use≥ 3 weeks	17 (4.2%)	6 (3.5%)	0.291
Recent lipid-lowering drugs use	26 (6.5%)	13 (7.5%)	0.642
Previous history of SAH	1 (0.2%)	0 (0%)	0.512
Coronary heart disease	42 (10.4%)	26 (15.0%)	0.116
Arterial stenosis	51 (12.7%)	22 (12.7%)	0.984
Diabetes	75 (18.6%)	29 (16.8%)	0.697
Drinking in small quantities	45 (11.2%)	15 (8.7%)	0.665
Excessive drinking	44 (10.9%)	19 (11.0%)	0.665
Previous history of transient ischemic attack	2 (0.5%)	1 (0.6%)	0.948
Previous history of ischemic stroke	26 (6.5%)	10 (5.8%)	0.948
Now ischemic attack	19 (4.7%)	5 (2.9%)	0.577
Now ischemic stroke	103 (25.6%)	43 (24.9%)	0.577
ELAPSS score	5.00 [1.00–10.00]	5.00 [1.00–10.50]	0.679
PHASES score	2.00 [1.00–4.00]	2.00 [1.00–5.00]	0.436
Radscore	3.96 [-15.07-12.45]	−0.07 [-15.03-18.88]	0.104

PLT, platelet count; WBC, white blood cell count; Hs-CRP, hypersensitive C-reactive protein; SAH, subarachnoid hemorrhage; Radscore, radiomics score.

3. Results

3.1. Random sampling

A total of 931 patients with confirmed IAs were included in this study. Among them, 192 (20.6%) patients with IAs diagnosed as ruptured IAs due to the occurrence of SAH during follow-up. 384 patients were randomly selected from 739 patients with unruptured IAs with a random number seed of 68439. The result of the Mann-Whitney *U* test showed that there was no significant difference in PHASES between the randomly selected sample and population (1.0 [1.0, 2.0] vs 1.0 [1.0, 2.0], $P = 0.596$). Finally, 576 patients with IAs, including 192 patients with ruptured IAs and 384 with unruptured IAs, were reviewed. There were 403 cases for training cohort and 173 cases for validation cohort.

3.2. Demographic and clinical characteristics

The cohort of 192 (192/576, 33.3%) patients with ruptured IA, were divided into training set (125 patients, 125/403, 31.0%) and the validation set (67 patients, 67/173, 38.7%). There were no significant differences in both the demographic and clinical characteristics between the training cohort and validation cohort, except neutrophil count ($P = 0.003$) and WBC ($P = 0.001$), (Table 1).

Through univariate analysis (Table 2), for the demographic data and medical history, age of patients in the rupture cohort was younger, and they less suffered from hypertension, coronary heart disease, diabetes, arterial stenosis and with recent use of lipid-

Table 2
Comparison of baseline characteristics between patients with ruptured IA group and unruptured IA group.

Variables	Ruptured IA Group (n = 125)	Unruptured IA Group (n = 278)	*P* value
Age (y)	58.12 ± 12.31	64.12 ± 11.88	<0.001
Male	45 (36.0%)	120 (43.2%)	0.176
Proximal diameter of parent artery (mm)	2.57 ± 0.80	3.42 ± 0.85	<0.001
Base width (mm)	2.80 [2.30–3.70]	2.70 [2.20–3.40]	0.166
Minor axis (mm)	3.50 [2.70–4.65]	2.10 [1.60–3.00]	<0.001
Major axis (mm)	4.80 [3.70–6.45]	2.60 [2.00–3.70]	<0.001
Irregular shape	57(45.6%)	14(5.0%)	<0.001
Regular shape	68 (54.4%)	264 (95.0%)	<0.001
Branching vessels	52 (41.6%)	51 (18.3%)	<0.001
Internal carotid artery	54 (43.2%)	226 (81.3%)	<0.001
Anterior communicating artery	32 (25.6%)	16 (5.8%)	<0.001
Middle cerebral artery	27 (21.6%)	21 (7.6%)	<0.001
Posterior cerebral artery	12 (9.6%)	15 (5.4%)	<0.001
PLT (10^9/L)	203.90 ± 67.83	194.11 ± 65.23	0.170
C-reactive protein (mg/L)	5.00 [5.00–11.96]	5.00 [0.50–5.00]	<0.001
WBC (10^9/L)	11.82 [9.26–15.04]	5.77 [4.83–7.34]	<0.001
Hs-CRP (mg/L)	4.23 [1.55–5.00]	1.24 [0.50–3.49]	<0.001
Monocyte percentage (%)	4.09 ± 1.96	6.40 ± 2.40	<0.001
Monocyte count (10^9/L)	0.43 [0.32–0.62]	0.37 [0.27–0.48]	0.001
Lymphocyte percentage (%)	7.00 [5.00–10.85]	24.25 [18.08–30.90]	<0.001
Lymphocyte count (10^9/L)	0.84 [0.62–1.08]	1.39 [1.05–1.74]	<0.001
Eosinophil percentage (%)	0.10 [0.00–0.15]	1.55 [0.80–2.60]	<0.001
Eosinophil count (10^9/L)	0.01 [0.00–0.02]	0.09 [0.05–0.16]	<0.001
Neutrophil percentage (%)	88.90[83.75–91.40]	66.20 [59.78–73.50]	<0.001
Neutrophil count (10^9/L)	10.68 [7.63–13.62]	3.78 [2.94–5.03]	<0.001
Smoking history	31 (24.8%)	69 (24.8%)	0.997
Hypertension	66 (52.8%)	177 (63.7%)	0.039
Recent Aspirin Use< 3 weeks	1 (0.8%)	5 (1.8%)	0.155
Recent Aspirin Use≥ 3 weeks	2 (1.6%)	15 (5.4%)	0.155
Recent lipid-lowering drugs use	2 (1.6%)	24 (8.6%)	0.008
Previous history of SAH	1 (0.8%)	0 (0%)	0.135
Coronary heart disease	2 (1.6%)	40 (14.4%)	<0.001
Arterial stenosis	5 (4.0%)	46 (16.5%)	<0.001
Diabetes	9 (7.2%)	66 (23.7%)	<0.001
Drinking in small quantities	10 (8.0%)	35 (12.6%)	0.400
Excessive drinking	14 (11.2%)	30 (10.8%)	0.400
Previous history of transient ischemic attack	0 (0%)	2 (0.7%)	0.052
Previous history of ischemic stroke	3 (2.4%)	23 (8.3%)	0.052
Now ischemic attack	0 (0)	19 (6.8%)	<0.001
Now ischemic stroke	13 (10.4%)	90 (32.4%)	<0.001
ELAPSS score	10.00 [5.00–15.50]	1.00 [1.00–5.00]	<0.001
PHASES score	4.00 [2.00–5.00]	1.00 [1.00–2.00]	<0.001
Radscore	16.36 [2.91–30.23]	−9.01 [-19.69–0.05]	<0.001

IA, intracranial aneurysm; PLT, platelet count; WBC, white blood cell count; Hs-CRP, hypersensitive C-reactive protein; SAH, subarachnoid hemorrhage; Radscore, radiomics score.

lowering drugs and the current history of ischemic attack or ischemic stroke. Among inflammatory features except PLT, the absolute and percentages of neutrophils, lymphocytes, monocytes, and eosinophils, as well as the WBC, c-reactive protein and hs-CRP were all associated with IA rupture. Except basal width, other 6 radiological features were associated with IA rupture. In the ruptured cohort, the major axis length and minor axis length of the IA were longer, the diameter of the parent artery was shorter, and there were more with vascular branches and irregular shape ($P < 0.05$).

Multiple regression indicated that in the training cohort, neutrophils percentage ($P = 0.006$), lymphocytes percentage ($P = 0.008$), monocyte percentage ($P = 0.007$), eosinophils percentage ($P = 0.002$) and hs-CRP ($P = 0.029$), as well as the proximal diameter of parent artery ($P = 0.005$) and shape ($P < 0.001$) were independent risk predictors of IA rupture (Table 3).

3.3. Radiomics analysis

The results of the intra-observer reproducibility showed that 99 (92.5%) radiomics features had ICCs >0.8, and the results of the inter-observer reproducibility showed that 101 (94.4%) radiomics features had ICCs >0.8.

During feature selection, 21 of the 107 radiomics features were retained after the T-test, with details described in the Supplementary Material. Subsequently, 7 features were obtained after Elastic-Net regression (Fig. 2A and B). The coefficient of each feature is shown in Fig. 2C.

The radiomics model was constructed by using these 7 features and the radscore for each patient was calculated as follows: Radscore = (shape_Elongation × −0.085927) + (firstorder_Maximum × −0.031062) + (firstorder_Skewness × −0.034820) + (glcm_ClusterShade × −0.004483) + (gldm_DependenceEntropy × 0.135926) +(glszm_ZonePercentage × −0.010569) + (ngtdm_Strength × −0.065108).

3.4. Model evaluation

The ROC curve of each model predicting ruptured IAs in the training and validation cohorts is summarized in Fig. 3A and B. The AUCs of the PHASES and ELAPSS were 0.729 and 0.797 in the training cohort, and 0.702 and 0.831 in the validation cohort.

The radscore model had an AUC of 0.814 and 0.805 in the training and validation cohort.

The inflammatory model constructed by five inflammatory features (neutrophils percentage, lymphocytes percentage, monocyte percentage, eosinophils percentage and hs-CRP) had an AUC of 0.935 and 0.927 in the training and validation cohort. We found the predictive ability of the inflammation model was significantly better than that of PHASES and ELAPSS.

The clinical model was constructed by combining 2 radiological features (parent artery diameter and shape) with 5 inflammatory features. Compared with the inflammatory model, the clinical model achieved a higher AUC of 0.970 and 0.952 in the training and validation cohort.

Combination of clinical model with radscore model, we got the C–R model. It achieved the best performance with an AUC of 0.975 and 0.962 in the training and validation cohort. In the validation cohort, the results of Delong tests showed that there was no statistical difference between the C–R model and the clinical model, the clinical model and the inflammatory model, and the radscore and the

Table 3
Multivariate analysis of baseline characteristics in the training cohort.

Variables	OR	95%CI	*P* value
Age (y)	0.96	0.93–1.00	0.053
Proximal diameter of parent artery (mm)	0.31	0.14–0.71	0.005
Minor axis (mm)	1.00	0.54–1.84	0.993
Major axis (mm)	1.12	0.71–1.76	0.628
shape	0.11	0.03–0.38	<0.001
Branching vessels	1.15	0.40–3.27	0.794
Anterior communicating artery	0.52	0.10–2.67	0.431
Middle cerebral artery	1.60	0.23–11.16	0.638
Posterior cerebral artery	0.49	0.08–3.00	0.437
C-reactive protein	0.98	0.96–1.01	0.148
WBC (10^9/L)	1.03	0.003–355.44	0.993
Hs-CRP (mg/L)	1.38	1.03–1.85	0.029
Monocyte percentage (%)	138.64	3.75–5120.07	0.007
Monocyte count (10^9/L)	2.30	0.01–959.11	0.786
Lymphocyte percentage (%)	132.03	3.61–4835.22	0.008
Lymphocyte count (10^9/L)	2.33	0.01–1033.74	0.785
Eosinophil percentage (%)	392.91	8.71–17725.97	0.002
Eosinophil count (10^9/L)	.000	0.001–194.69	0.159
Neutrophil percentage (%)	158.15	4.32–5786.05	0.006
Neutrophil count (10^9/L)	1.48	0.003–680.73	0.900
Hypertension	1.38	0.51–3.75	0.527
Recent lipid-lowering drugs use	1.07	0.06–17.98	0.962
Coronary heart disease	2.39	0.13–42.63	0.553
Diabetes	0.87	0.19–4.00	0.856

OR, indicates odds ratio; CI, confidence interval; Hs-CRP, hypersensitive C-reactive protein.

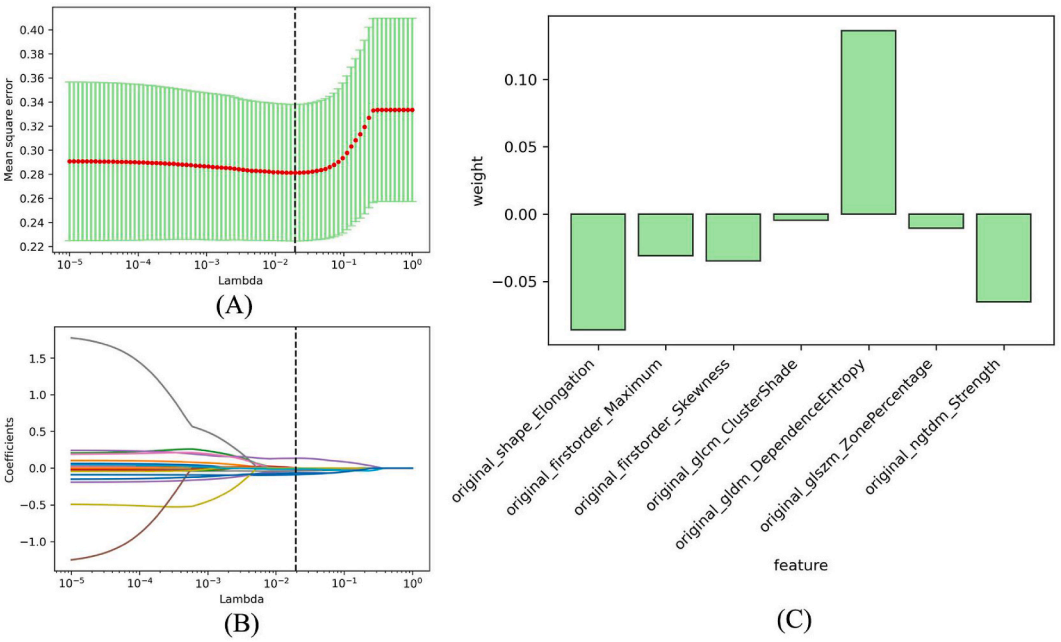

Fig. 2. Feature selection with Elastic-Net regression. (A) Tuning parameter (lambda) selection in the Elastic-Net regression using 10-fold cross-validation. (B) Elastic-Net regression coefficient analysis of the 21 radiomics features. Each coloured line represents the coefficient of each feature. (C) The X-axis represents individual radiomics features, and their coefficients in the Elastic-Net regression analysis are plotted on the Y-axis.

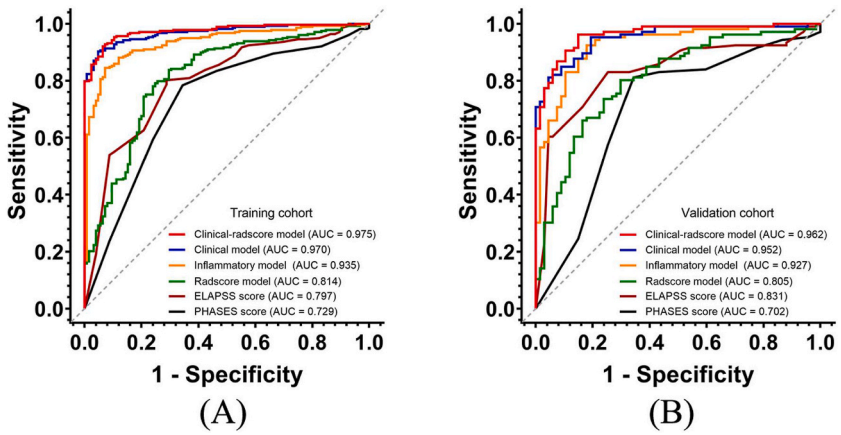

Fig. 3. ROC curves of four models (radscore, inflammatory, clinical, and C–R model) and two scores (PHASES and ELAPSS scores). (A) The ROC curves of four models and two scores for predicting IA rupture risk in the training cohort. (B) The ROC curves of four models and two scores for predicting IA rupture risk in the validation cohort.

ELAPSS, while there were statistical differences among the other models ($P < 0.05$), (Table 4).

Using the C–R model, we further developed a multi-predictor nomogram with 8 independent predictors (shape, proximal diameter of the parent artery, neutrophils percentage, lymphocytes percentage, monocyte percentage, eosinophils percentage, hs-CRP and

Table 4
Delong tests for predictive performances between different models in the validation cohort.

Items	C–R model	Clinical model	Inflammatory model	Radscore	PHASES	ELAPSS
C–R model	–	0.1487	0.0382	<0.0001	<0.0001	<0.0001
Clinical model	–	–	0.1289	<0.0001	<0.0001	0.0001
Inflammatory model	–	–	–	0.0023	<0.0001	0.0112
Radscore	–	–	–	–	0.0274	0.3308
PHASES	–	–	–	–	–	0.0010

radscore) to estimate the risk of IA rupture (Fig. 4). The DeLong test showed that the AUCs of the C–R model between the training and validation cohorts ($P = 0.378$) was not significantly different. In addition, the calibration curves showed the C–R nomogram had prediction consistency in the training and validation cohort (Fig. 5A and B). The results of DCA showed the C–R nomogram had good clinical benefits in the training and validation cohort (Fig. 6A and B).

4. Discussion

In our study, we used a random sampling to balance the number of rupture and unruptured IAs, which made our models stable and performed better. Four models were built to verify their predictive abilities for IA rupture. Finally, we found 5 inflammatory features, 2 radiological features and 7 radiomics features could be applied as independent predictors for IA rupture. In particular, the inflammatory indicators performed very well and could act as a new indicator for the prediction. Based on clinically-available baseline characteristics, objectively and effectively assessing the risk of IA rupture for individual is practical.

In recent years, studies have attempted to apply radiomics features to assess risk of IA rupture and have shown good predictive performance [16,20]. Consent with the previous studies [16,20], we found that radiomics score predicted IA rupture well with higher predictive performance than the PHASES and ELAPSS scores. The radiomics features of IAs can be acted as predictors for predicting IA rupture [16,18]. In addition, the predictive performance of our radiomics model (an AUC of 0.805 in validation cohort) was close to that of the radiomics model built by Zhu's study (an AUC of 0.817 in the validation cohort) [17]. In this study, we extracted 107 radiomics features from each IA. Among them, the texture features performed the best in predicting the risk of IA rupture, which keeps in line with previous studies [16,17]. Those features reflected the intensity level of voxel spatial distribution and the coarseness of texture. The heterogeneity of these voxel distributions suggested the density heterogeneity of the aneurysm lumen on CTA images. This can be understood as abnormal intraluminal hemodynamics in IAs, it causes inhomogeneous distribution of contrast agent within the aneurysm lumen [16,21]. In addition, the radiomics features of Maximum, Skewness and Elongation described the IAs' shape and texture characteristics under the microcosmic view [17]. They can be acted as shape descriptors for predicting IA rupture better [16].

We also developed a clinical model by using radiological and inflammatory features, which had a satisfactory prediction. It is generally believed that the degeneration of vascular vessel wall and abnormal aneurysm morphology are related to IA rupture. Chen's study also found that the structural factors of the arterial wall play an important role in the formation and development of IA, and arterial bifurcation with medial gap were prone to be damaged [22]. Our study showed the relevant results. In our study, IA shape and diameter of parent artery were proven to be independent predictors, which had also been reported by other researchers [23,24]. The structure of the parent artery and the size and shape of the aneurysm strongly influence its hemodynamics, and this will further affect the risk of IA rupture [12,25,26]. At the same time, the irregular shape also can change the wall shear stress (WSS), and both high and low WSS will increase the rupture risk of IAs [25].

The level of inflammation factors inside IAs in ruptured IAs patients is higher than that in their peripheral blood, and the level of it in the peripheral blood of IAs (the ruptured and unruptured) is higher than that in the healthy cases [27]. Inflammatory indicators in peripheral blood indirectly reflect inflammation in IA to some extent. The inflammation is triggered by abnormal hemodynamics and produces endothelial dysfunction, which results in a chronic inflammatory reaction [28]. A series of processes, including progressive vascular wall remodeling, myointimal hyperplasia and extracellular matrix (ECM) degradation promote the formation and progression of IAs. This causes the transformation of the aneurysm wall. And it makes IAs to form a specific histological type that is easy to rupture [25]. And for the hs-CRP, it has the strongest correlation with cardiovascular risk. It can activate complement system and produces a large number of inflammatory mediators and releases oxygen free radicals, resulting in vascular intimal damage, vasospasm and other

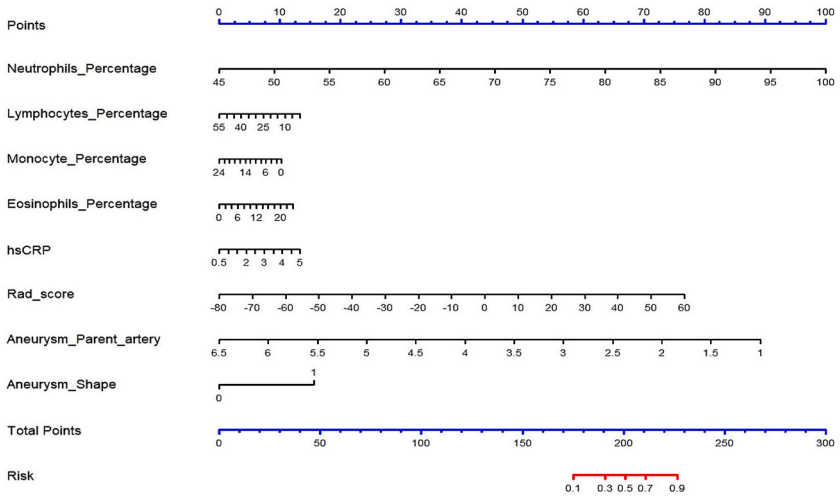

Fig. 4. A C–R nomogram for assessing the risk of IA rupture. The nomogram is used by first summing the points corresponding to all predictors and then find the corresponding risk of IA rupture.

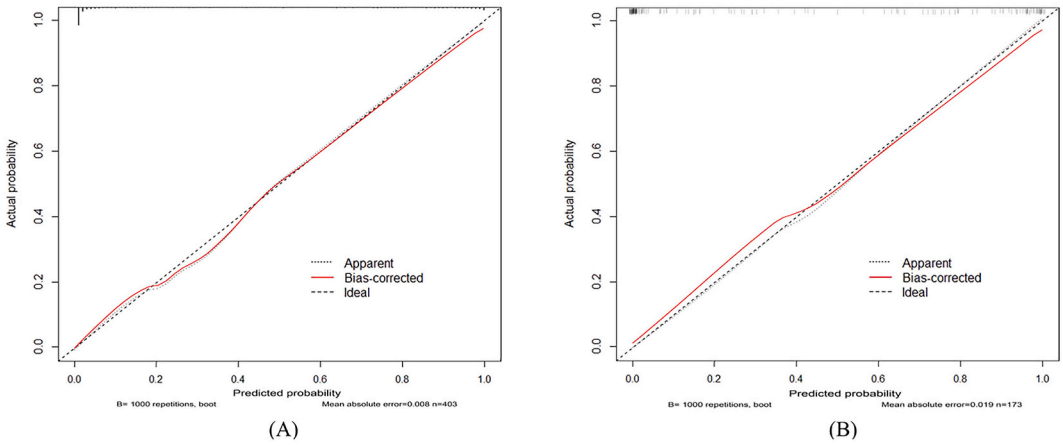

Fig. 5. Calibration curves of the C–R model. (A) The calibration curve of the C–R model for predicting IA rupture risk in the training cohort. (B) The calibration curve of the C–R model for predicting IA rupture risk in the validation cohort.

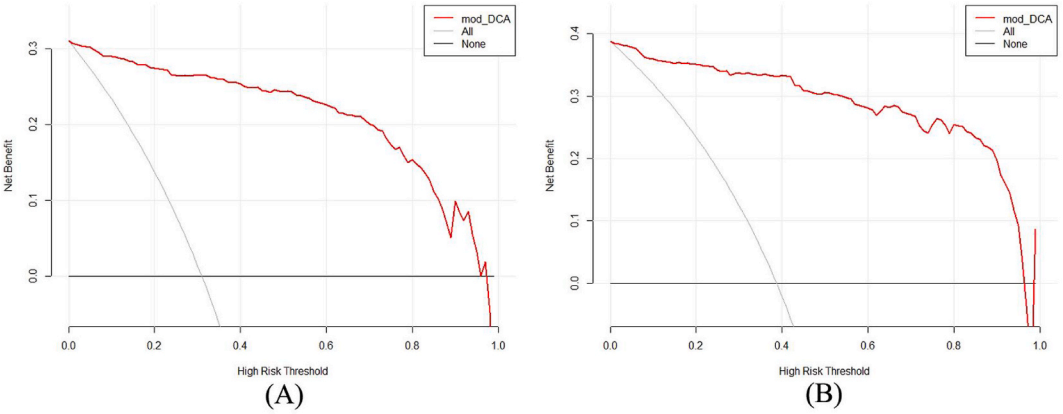

Fig. 6. Decision curves of the C–R model. (A)The decision curve of the C–R model for predicting IA rupture risk in the training cohort. (B) The decision curve of the C–R model for predicting IA rupture risk in the validation cohort.

adverse consequences [29].Although inflammatory indicators are strongly associated with both IA formation as well as rupture [30], just few researches use those indicators for IA rupture prediction [31]. In our study, we surprisingly found that 5 inflammatory indicators in peripheral blood were strongly associated with IA rupture, and the corresponding inflammatory model had excellent predictive performance.

As a very important part of inflammation, leukocyte plays also very important role in IA rupture. A study by Zhang et al. had proven ratio of neutrophils to lymphocytes and hs-CRP could predict the risk of IA rupture, with an AUC of 0.791 and 0.817 respectively [14]. Our research also revealed the similar results, with neutrophils and eosinophils positively associated with the risk of IA rupture, and lymphocytes and monocytes negatively associated with the risk of IA rupture.

Neutrophils accelerates the degeneration of vascular wall by providing inflammatory microenvironment and producing destructive protease, and this promotes the rupture of the injured site [12,32]. Eosinophils releases particles and leads to tissue damage [33]. Monocytes infiltrates wall of blood vessels and develops into macrophages during inflammation. Macrophages and lymphocytes participate in the formation and development of IAs by degrading ECM and remodeling blood vessels [12,34]. In short, the release of inflammatory factors and leukocyte infiltration will damage the vascular wall and make the risk of IA rupture higher. Compared with the model in Zhang's study [14], our inflammation model achieved better performance, with an AUC of 0.927 in the validation cohort. The reason may be that we included more inflammatory features and used logistic regression.

Combined models generally have better prediction ability, due to the inclusion of more comprehensive predictors. A previous study found that the use of radiological features could significantly improve the performance for IA rupture prediction [16]. In addition, Zhu's study had found that the combined model had a higher AUC in predicting IA rupture compared to clinical or morphological, radiomics models [17]. Our C–R model was constructed based on 5 inflammatory features, 2 radiological features and radiomics score, and achieved excellent predictive performance. This can be interpreted that more independent indicators inclusion improved the predictive performance. Based on C–R model, we also developed a C–R nomogram. It directly and visually demonstrated the

assessment for IA rupture. This made the evaluation for IA rupture more practical and convenient.

However, this study has some limitations. Firstly, this is a retrospective cross-sectional study. In the future, we will follow patients with unruptured IA longitudinally to further optimize the prediction model. Secondly, inflammatory features in peripheral blood do not directly reflect inflammatory infiltration of the IA wall, and this needs the study of inflammatory factors inside IA wall further. Thirdly, multiple IAs and external validation were necessary to improve the applicability of our C–R model.

In conclusion, the radiomics and radiological features of IAs, as well as the inflammatory features in peripheral blood can predict the risk of rupture of IAs well, and the visualized C–R nomogram provides an accurate and practical risk assessment for IA rupture. It can help clinicians to stratify the management of unruptured IAs and develop individualized treatment and follow-up plans for them.

Data availability statement

Data will be made available on request.

Ethical approval

This study was approved by the Ethics Committee of the Second Affiliated Hospital of Chongqing Medical University (No. [2023] 108), and waived the requirement of written informed consent for participation.

Sources of support

This study was sponsored by Natural Science Foundation of Chongqing, China (Grant No.CSTB2022NSCQ-MSX0116).

CRediT authorship contribution statement

Wenjie Li: Conceptualization, Data curation, Investigation, Methodology, Writing - original draft, Writing - review & editing. **Xiaojia Wu:** Conceptualization, Methodology, Supervision, Writing – original draft, Writing – review & editing. **Jing Wang:** Data curation. **Tianxing Huang:** Investigation. **Lu Zhou:** Data curation. **Yu Zhou:** Investigation. **Yuanxin Tan:** Investigation. **Weijia Zhong:** Conceptualization, Supervision, Validation, Writing – review & editing. **Zhiming Zhou:** Conceptualization, Funding acquisition, Methodology, Writing – review & editing.

Declaration of competing Interest

The authors declare that they have no known competing financial interests or personal relationships that could have appeared to influence the work reported in this paper.

Appendix A. Supplementary data

Supplementary data to this article can be found online at https://doi.org/10.1016/j.heliyon.2023.e20718.

References

[1] R. Jabbarli, et al., Risk factors for and clinical consequences of multiple intracranial aneurysms: a systematic review and meta-analysis, Stroke 49 (4) (2018) 848–855.
[2] Z. Xu, et al., Intracranial aneurysms: pathology, genetics, and molecular mechanisms, NeuroMolecular Med. 21 (4) (2019) 325–343.
[3] M. Korja, et al., Natural history of ruptured but untreated intracranial aneurysms, Stroke 48 (4) (2017) 1081–1084.
[4] N. Etminan, et al., European Stroke Organisation (ESO) guidelines on management of unruptured intracranial aneurysms, Eur Stroke J 7 (3) (2022) V.
[5] G. Boulouis, et al., Unruptured intracranial aneurysms: an updated review of current concepts for risk factors, detection and management, Rev. Neurol. 173 (9) (2017) 542–551.
[6] G. Rinkel, Natural history, epidemiology and screening of unruptured intracranial aneurysms, Rev. Neurol. 164 (10) (2008) 781–786.
[7] E. Hitchcock, W. Gibson, A review of the genetics of intracranial berry aneurysms and implications for genetic counseling, J. Genet. Counsel. 26 (1) (2017) 21–31.
[8] D. Backes, et al., ELAPSS score for prediction of risk of growth of unruptured intracranial aneurysms, Neurology 88 (17) (2017) 1600–1606.
[9] J. Greving, et al., Development of the PHASES score for prediction of risk of rupture of intracranial aneurysms: a pooled analysis of six prospective cohort studies, Lancet Neurol. 13 (1) (2014) 59–66.
[10] M. Sánchez van Kammen, et al., External validation of the ELAPSS score for prediction of unruptured intracranial aneurysm growth risk, J Stroke 21 (3) (2019) 340–346.
[11] B. Neyazi, I. Sandalcioglu, H. Maslehaty, Evaluation of the risk of rupture of intracranial aneurysms in patients with aneurysmal subarachnoid hemorrhage according to the PHASES score, Neurosurg. Rev. 42 (2) (2019) 489–492.
[12] F. Signorelli, et al., Hemodynamic stress, inflammation, and intracranial aneurysm development and rupture: a systematic review, World neurosurgery 115 (2018) 234–244.
[13] H.K. Kim, et al., The clinical significance of peripheral blood cell ratios in patients with intracranial aneurysm, Front. Neurol. 13 (2022), 1080244.
[14] B. Zhang, et al., Clinical application values of neutrophil-to-lymphocyte ratio in intracranial aneurysms, Aging 13 (4) (2021) 5250–5262.
[15] P. Lambin, et al., Radiomics: extracting more information from medical images using advanced feature analysis, Eur. J. Cancer 48 (4) (2012) 441–446.

[16] C. Ou, et al., A preliminary investigation of radiomics differences between ruptured and unruptured intracranial aneurysms, Eur. Radiol. 31 (5) (2021) 2716–2725.
[17] D. Zhu, et al., Classifying ruptured middle cerebral artery aneurysms with a machine learning based, radiomics-morphological model: a multicentral study, Front. Neurosci. 15 (2021), 721268.
[18] Q. Liu, et al., Prediction of aneurysm stability using a machine learning model based on PyRadiomics-derived morphological features, Stroke 50 (9) (2019) 2314–2321.
[19] P. Bijlenga, et al., PHASES score for the management of intracranial aneurysm: a cross-sectional population-based retrospective study, Stroke 48 (8) (2017) 2105–2112.
[20] C. Ludwig, et al., Performance of Radiomics derived morphological features for prediction of aneurysm rupture status, J. Neurointerventional Surg. 13 (8) (2021) 755–761.
[21] A. Aghayev, et al., Common first-pass CT angiography findings associated with rapid growth rate in abdominal aorta aneurysms between 3 and 5 cm in largest diameter, AJR Am. J. Roentgenol. 210 (2) (2018) 431–437.
[22] B. Chen, et al., Medial gap: a structural factor at the arterial bifurcation aggravating hemodynamic insult, J. Neuropathol. Exp. Neurol. 81 (4) (2022) 282–290.
[23] S. Tanioka, et al., Machine learning classification of cerebral aneurysm rupture status with morphologic variables and hemodynamic parameters, Radiol Artif Intell 2 (1) (2020), e190077.
[24] Y. Duan, et al., Relationship between middle cerebral parent artery asymmetry and middle cerebral artery aneurysm rupture risk factors, J. Neurosurg. 132 (4) (2019) 1174–1181.
[25] A. Giotta Lucifero, et al., Shedding the light on the natural history of intracranial aneurysms: an updated overview, Medicina 57 (8) (2021).
[26] P.M. Munarriz, et al., Basic principles of hemodynamics and cerebral aneurysms, World Neurosurg 88 (2016) 311–319.
[27] A.M. de Korte, et al., Elevation of inflammatory S100A8/S100A9 complexes in intracranial aneurysms, J. Neurointerventional Surg. 12 (11) (2020) 1117–1121.
[28] H. Kataoka, et al., Hemodynamic and histopathological changes in the early phase of the development of an intracranial aneurysm, Neurol. Med.-Chir. 60 (7) (2020) 319–328.
[29] A. Denegri, G. Boriani, High sensitivity C-reactive protein (hsCRP) and its implications in cardiovascular outcomes, Curr. Pharmaceut. Des. 27 (2) (2021) 263–275.
[30] J.W. Barrow, et al., The role of inflammation and potential use of sex steroids in intracranial aneurysms and subarachnoid hemorrhage, Surg. Neurol. Int. 9 (2018) 150.
[31] K. Shimizu, et al., Intracranial aneurysm as a macrophage-mediated inflammatory disease, Neurol. Med.-Chir. 59 (4) (2019) 126–132.
[32] C. Tecchio, M.A. Cassatella, Neutrophil-derived chemokines on the road to immunity, Semin. Immunol. 28 (2) (2016) 119–128.
[33] N.G. Kounis, et al., White blood cell counts, leukocyte ratios, and eosinophils as inflammatory markers in patients with coronary artery disease, Clin. Appl. Thromb. Hemost. 21 (2) (2015) 139–143.
[34] S. Muhammad, et al., Vascular macrophages as therapeutic targets to treat intracranial aneurysms, Front. Immunol. 12 (2021), 630381.